

A Closer Look at the Spectroscopic Properties of Possible Reaction Intermediates in Wild-Type and Mutant (*E*)-4-Hydroxy-3-methylbut-2-enyl Diphosphate Reductase

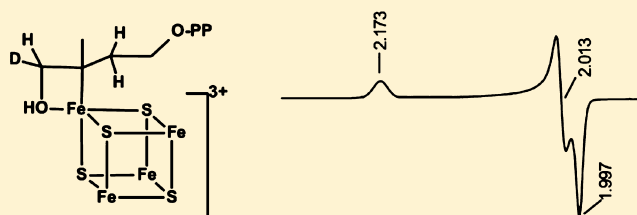
Weiya Xu,[†] Nicholas S. Lees,[‡] Dominique Hall,[†] Dhanushi Welideniya,[†] Brian M. Hoffman,[‡] and Evert C. Duin^{*,†}

[†]Department of Chemistry and Biochemistry, Auburn University, Auburn, Alabama 36849, United States

[‡]Department of Chemistry, Northwestern University, Evanston, Illinois 60208, United States

S Supporting Information

ABSTRACT: (*E*)-4-Hydroxy-3-methylbut-2-enyl diphosphate reductase (IspH or LytB) catalyzes the terminal step of the MEP/DOXP pathway where it converts (*E*)-4-hydroxy-3-methylbut-2-enyl diphosphate (HMBPP) into the two products, isopentenyl diphosphate and dimethylallyl diphosphate. The reaction involves the reductive elimination of the C4 hydroxyl group, using a total of two electrons. Here we show that the active form of IspH contains a [4Fe-4S] cluster and not the [3Fe-4S] form. Our studies show that the cluster is the direct electron source for the reaction and that a reaction intermediate is bound directly to the cluster. This active form has been trapped in a state, dubbed FeS_A, that was detected by electron paramagnetic resonance (EPR) spectroscopy when one-electron-reduced IspH was incubated with HMBPP. In addition, three mutants of IspH have been prepared and studied, His42, His124, and Glu126 (*Aquifex aeolicus* numbering), with particular attention paid to the effects on the cluster properties and possible reaction intermediates. None of the mutants significantly affected the properties of the [4Fe-4S]⁺ cluster, but different effects were observed when one-electron-reduced forms were incubated with HMBPP. Replacing His42 led to an increased *K_M* value and a much lower catalytic efficiency, confirming the role of this residue in substrate binding. Replacing the His124 also resulted in a lower catalytic efficiency. In this case, however, the enzyme showed the loss of the [4Fe-4S]⁺ EPR signal upon addition of HMBPP without the subsequent formation of the FeS_A signal. Instead, a radical-type signal was observed in some of the samples, indicating that this residue plays a role in the correct positioning of the substrate. The incorrect orientation in the mutant leads to the formation of substrate-based radicals instead of the cluster-bound intermediate complex FeS_A. Replacing the Glu126 also resulted in a lower catalytic efficiency, with yet a third type of EPR signal being detected upon incubation with HMBPP. ³¹P and ²H ENDOR measurements of the FeS_A species incubated with regular and ²H-C4-labeled HMBPP reveal that the substrate binds to the enzyme in the proximity of the active-site cluster with C4 adjacent to the site of linkage between the FeS cluster and HMBPP. Comparison of the spectroscopic properties of this intermediate to those of intermediates detected in (*E*)-4-hydroxy-3-methylbut-2-enyl diphosphate synthase and ferredoxin:thioredoxin reductase suggests that HMBPP binds to the FeS cluster via its hydroxyl group instead of a side-on binding as previously proposed for the species detected in the inactive Glu126 variant. Consequences for the IspH reaction mechanism are discussed.



The (*E*)-4-hydroxy-3-methylbut-2-enyl diphosphate reductase (IspH or LytB) catalyzes the terminal step of the 2-C-methyl-D-erythritol 4-phosphate/1-deoxy-D-xylulose 5-phosphate (MEP/DOXP) pathway, the conversion of (*E*)-4-hydroxy-3-methylbut-2-enyl diphosphate (HMBPP) into the two products, isopentenyl diphosphate (IPP) and dimethylallyl diphosphate (DMAPP) (Figure 1).^{1–3} IspH and other enzymes in the MEP/DOXP pathway are currently in the spotlight because the pathway is one of two that are found in nature for the synthesis of IPP and DMAPP. These are the building blocks for the large group of molecules called isoprenoids or terpenes, which include biologically essential compounds like vitamins, cholesterol, steroid hormones, carotenoids, and quinines.^{4,5} Mammals use the mevalonate pathway to synthesize the

isoprene precursors, while eubacteria and apicomplexan parasites use the MEP/DOXP pathway as the sole pathway for isoprene synthesis.⁴ Several of these microorganisms are pathogens, causing, for example, malaria, tuberculosis, anthrax, plague, cholera, and venereal diseases.⁶ This makes the MEP/DOXP pathway an attractive target for the development of new anti-infective drugs. Because this pathway is not present in humans, these inhibitors should demonstrate very low toxicity. Fosmidomycin, an inhibitor of the enzyme DOXP reductoisomerase in the MEP/DOXP pathway, can be used for the

Received: January 26, 2012

Revised: May 30, 2012

Published: May 30, 2012



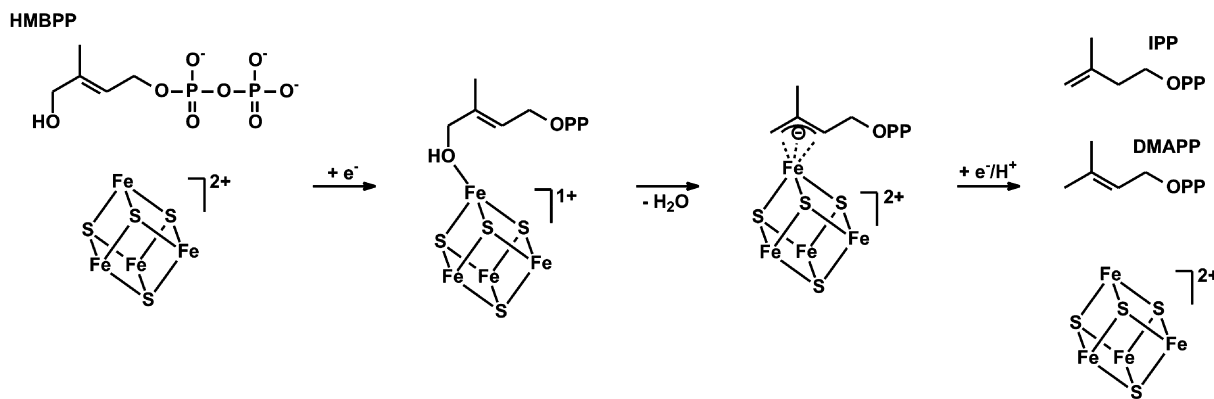


Figure 1. IspH mechanism I. Reaction mechanism for the conversion of HMBPP by IspH. See the text for details.

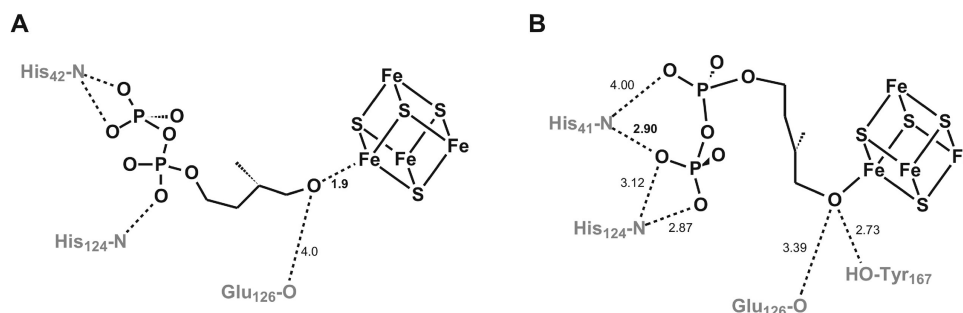


Figure 2. Binding of HMBPP in the active site of IspH. (A) Modulation of HMBPP in the open site of *A. aeolicus* IspH. (B) HMBPP bound in the crystal structure of *E. coli* IspH. Note that the numbering is different for the enzymes from the two organisms.

treatment of acute uncomplicated *Plasmodium falciparum* infections (malaria), but an overall cure rate of 95% in clinical studies was achieved only when fosmidomycin was tested in combination with clindamycin, showing the need for compounds with higher efficacy.^{7–13} Research efforts focus on finding fosmidomycin analogues that can work as stand-alone drugs^{14–22} but also on finding inhibitors for the other enzymes in the MEP/DOXP pathway, which could be used in combination with fosmidomycin. Isoprenoids also have biotechnological applications as drugs, flavors, pigments, perfumes, and agrochemicals. A detailed knowledge of the mechanisms of the enzymes and regulation of the pathway could or is already benefitting the biotechnological production of commercially interesting isoprenoids, such as carotenoids,^{23,24} and Taxol.²⁵ The MEP/DOXP pathway is also present in the plastids of plants, and targeting this pathway could result in the development of novel herbicides that are less harmful to humans.^{26,27}

The IspH protein is an iron–sulfur cluster-containing enzyme. There is some confusion, however, about whether the active-site cluster is a [4Fe-4S] or [3Fe-4S] cluster. This is mainly due to the crystal structures of IspH proteins from *Aquifex aeolicus* and *Escherichia coli*. The *A. aeolicus* enzyme was crystallized in a relatively “open” form and contained a [3Fe-4S] cluster,²⁸ whereas the *E. coli* enzyme, which was crystallized under several different conditions, exhibited “closed” structures that contained either a [3Fe-4S] cluster or a [4Fe-4S] cluster.^{29–31} The structural data place the substrate HMBPP and the iron–sulfur cluster very close to each other. In light of the catalytic reaction, which involves the reductive elimination of the hydroxyl group, the cluster is the most logical direct source of the needed electrons. The redox potential of a three-Fe cluster, however, is too high for it to fulfill such a role. More

importantly, the only structure that is obtained with bound HMBPP contains a [4Fe-4S] cluster. The fourth iron in this cluster features a typical Fe–O bond distance of 2.0 Å for the oxygen of the hydroxyl group of HMBPP. This would imply a direct role of the four-Fe cluster in the reaction mechanism, in line with a recent proposal where the binding of HMBPP with its hydroxyl group to the [4Fe-4S] cluster is the starting point of the reaction.^{32,33} In this hypothetical mechanism (Figure 1), the transfer of the first electron from the cluster to bound HMBPP results in the removal of the hydroxyl group, which leaves as water, and the formation of an allyl anion that could be stabilized by direct or indirect σ/π interaction with the cluster. This type of interaction was proposed on the basis of the spectroscopic properties of a paramagnetic species detected in an IspH mutant (E126Q).³² It was further proposed that the cluster with the bound reaction intermediate receives another electron and the concomitant protonation results in the formation and release of either IPP or DMAPP. The ratio of these products appears to be determined kinetically³¹ and can be anywhere between 4:1 and 6:1, depending on the origin of the enzyme (*A. aeolicus*, *E. coli*, or *P. falciparum*) or enzyme type (as-isolated or reconstituted).^{1–3,34} Electrons can be donated by the natural flavodoxin/flavodoxin reductase/NADH system (*E. coli*)^{35–37} or ferredoxin (*P. falciparum*)³⁸ or by artificial donors, including photoactivated deazaflavin³⁹ and dithionite.¹

This work reveals a linear dependency of WT enzyme activity and [4Fe-4S] cluster content, confirming that protein containing this cluster type represents the active form of the enzyme. It further reports that when a one-electron-reduced form of the WT enzyme is incubated with HMBPP a new paramagnetic species is trapped. The properties of this species indicate that it is an intermediate that forms as a stage on the

enzyme reaction pathway. The spectroscopic properties of this intermediate formed in the WT enzyme, denoted FeS_A , are different from those of the species detected in the E126Q mutant, and the behavior of the species formed in the mutant enzyme suggests it may not lie along the reaction pathway. Given the likely significance of the FeS_A state, it has been studied by EPR and ENDOR spectroscopies.

A third topic investigated is the effects of site-directed mutagenesis on protein activity and cluster properties. From the crystal structures, the amino acids that probably play a role in the binding of substrate and in the reaction mechanism can be deduced. The structure of IspH is quite flat and displays a cloverleaf motif built up of α/β domains that surround a central iron–sulfur cluster. In the open *A. aeolicus* structure,²⁸ there is a pronounced cavity ($\sim 10 \text{ \AA} \times 20 \text{ \AA}$) located at the front side. The $[\text{3Fe-4S}]$ cluster is found at the bottom of the crevice. Computational studies, with a four-Fe cluster instead of the detected three-Fe cluster, indicated that the diphosphate group of HMBPP is most likely coordinated by His42 and His124 (*A. aeolicus* numbering) (Figure 2A).²⁸ The highly conserved Glu126 seemed to be the only candidate that could participate in acid–base chemistry. The studies indicated a possible interaction of the hydroxyl group of HMBPP with the unique iron of the active-site cluster. The *E. coli* structure with bound HMBPP showed a slightly different picture (Figure 2B).³⁰ In this case, the enzyme is in the closed conformation and HMBPP is trapped inside. Most of the conserved amino acids do not change position in comparison to those of the open form, except for His42 (His41 in *E. coli*), which is shifted $\sim 4 \text{ \AA}$.³⁰ In this structure, HMBPP has an almost cyclic form and the orientation of the diphosphate group is different from that in the *A. aeolicus* model by 180° . As mentioned, the hydroxyl group is bound to the fourth iron of the iron–sulfur cluster. The structure also shows a possible relay system in which the proton for the last reaction step would come from a water molecule present in most structures that is hydrogen bonded to Glu126, which in turn can pass the proton to Tyr167, which is in a better position to donate a proton to the allyl anion intermediate.

Confirmation of the assigned roles of these amino acids in the binding of HMBPP and in the reaction mechanism has to come from site-directed mutagenesis studies. Some of these sites have been probed in this fashion,^{29,32} but those studies lack detailed information about the kinetic and spectroscopic properties of the produced mutants. Here we present studies of the enzymatic function of IspH mutated at the His42, His124, or Glu126 position. The characteristics of “reaction intermediates” induced when the one-electron-reduced mutant enzyme is incubated with HMBPP are also discussed.

From a comparison of the catalytic properties of WT and mutant IspH and of the spectroscopic studies of the paramagnetic species formed upon incubation of the one-electron-reduced forms of the WT and mutant enzyme with HMBPP, a clearer picture of the role of the three amino acids in cluster properties, substrate binding, and the reaction mechanism of IspH emerges.

MATERIALS AND METHODS

Materials. Elemental ^{57}Fe (95% enrichment) was from WEB Research Co. $^{57}\text{FeCl}_3$ was prepared by reacting solid ^{57}Fe in 37% HCl. After all iron had reacted, the pH was adjusted to 4–5 with NaOH. ^2H -labeled HMBPP was donated by E. Oldfield's group at the University of Illinois (Urbana, IL).

Dithionite was from Fisher Scientific. All gases and gas mixtures were from Airgas.

Anaerobic conditions are required for all experiments. This was achieved by performing all purification steps, sample handling, and experiments in a glovebox (Coy Laboratory Products, Inc.) with an atmosphere of 95% N_2 and 5% H_2 . All buffers and solutions used in the procedures were degassed by being boiled under a nitrogen atmosphere and subsequently cooled under vacuum for 2–12 h.

Expression and Purification. The expression plasmids for WT IspH from *A. aeolicus* and *P. falciparum* were provided by the H. Jomaa's group at the Justus-Liebig University (Giessen, Germany). The expression plasmid for WT IspH from *E. coli* was provided by M. Groll's group at the Technical University Munich (Munich, Germany). Plasmids with site-directed mutants of IspH from *A. aeolicus* were provided by E. Oldfield's group. Wild-type IspH protein (from *A. aeolicus*, *E. coli*, and *P. falciparum*) and mutated IspH proteins from *A. aeolicus* were overexpressed successfully in *E. coli* XL-1 blue cells. All IspH proteins contained a His₆ tag and were purified by immobilized nickel affinity chromatography.

The cell cultures were started with a single colony from an LB-Amp plate that was transferred into SOC medium containing 100 mg/L ampicillin and 300 μM FeCl_3 . The cultures were incubated at 37°C while being shaken. For ^{57}Fe isotope-enriched protein, $^{57}\text{FeCl}_3$ was used. For IspH from *A. aeolicus* (both wild type and mutants) and *P. falciparum*, anhydrotetracycline was used as an inducer. For IspH from *E. coli*, IPTG was used as an inducer. The cells were harvested by centrifugation at 5500 rpm for 30 min (Sorvall RC-SB Refrigerated Superspeed Centrifuge, Sorvall GS-3 Rotor, Du Pont Instrument). The cell pellets were stored at -80°C until they were needed.

The purification and subsequent sample handling steps were performed in the Coy box. Buffer containing 50 mM Tris-HCl and 100 mM NaCl (pH 8.0) was used to resuspend the cell pellets. The cells were disintegrated by sonication, followed by centrifugation at 35000 rpm for 30 min (Beckman XL-70 Ultracentrifuge, YPE 45 Ti Rotor, Beckman Coulter, Inc.). The *A. aeolicus* cell extract was subsequently incubated at 65°C in a water bath for 30 min, followed by a second centrifugation step after which the supernatant was loaded on the HisTrap Affinity column (Pharmacia, GE Healthcare). The heat treatment was skipped for the *P. falciparum* and *E. coli* enzymes. Protein was eluted with increasing amounts of imidazole in the buffer. Enzyme eluted at an imidazole concentration of 250 mM. The main fractions were collected and used freshly. Unless indicated, all experiments were performed in 50 mM Tris-HCl and 100 mM NaCl (pH 8.0). The protein samples were judged to be pure ($>95\%$) based on sodium dodecyl sulfate–polyacrylamide gel electrophoresis (not shown).

Determination of Protein and Iron Levels. The enzyme concentration was determined by the Bradford method⁴⁰ or directly based on the absorbance at 280 nm depending on Tyr and Trp content: $\epsilon = 26930 \text{ M}^{-1} \text{ cm}^{-1}$ for *A. aeolicus* (32 kDa), $\epsilon = 20190 \text{ M}^{-1} \text{ cm}^{-1}$ for *E. coli* (35 kDa), and $\epsilon = 41260 \text{ M}^{-1} \text{ cm}^{-1}$ for *P. falciparum* (37 kDa). The determination of the iron concentration was conducted with a rapid ferrozine-based colorimetric method.⁴¹ Adventitiously bound iron was removed by running the protein samples over a Chelex 100 column (Bio-Rad).

Reconstitution. Most of the IspH samples exhibited substoichiometric amounts of the active-site $[\text{4Fe-4S}]$ cluster.

Reconstitution of the cluster was achieved by incubation overnight with dithiothreitol (≥ 5 mM), FeCl_3 (5 times the protein concentration), and Na_2S (5 times the protein concentration) in 50 mM Tris-HCl (pH 8.0). The samples were centrifuged in an Eppendorf centrifuge (4500 rpm for 5 min) to remove the black, iron-containing precipitate. The supernatant was desalted by running it over a PD 10 column. The eluted protein was used directly.

Kinetic Studies. The kinetic studies for WT and mutant IspH were performed at room temperature with the reaction mixture containing dithionite, methyl viologen, and substrate. The activity of IspH was determined by monitoring the oxidation of dithionite-reduced methyl viologen at 732 nm ($\epsilon_{732} = 2200 \text{ M}^{-1} \text{ cm}^{-1}$) or 603 nm ($\epsilon_{603} = 13600 \text{ M}^{-1} \text{ cm}^{-1}$). The concentration of substrate HMBPP was varied from 0 to 500 μM .

UV–visible absorption spectra were recorded under anaerobic conditions using an Ocean Optics USB 2000 miniature fiber optic spectrometer inside the glovebox or using stoppered cuvettes in an HP 8451A UV–visible spectrophotometer or an Agilent 8453 UV–visible spectrophotometer.

Circular Dichroism (CD) Spectroscopy. CD spectroscopy was conducted to check the proper folding of the mutant enzymes. As-isolated enzyme was washed with 5 mM phosphate buffer (pH 8.0) to remove both imidazole and the Tris buffer. An aliquot was transferred into a 0.1 mm cuvette that was capped inside the glovebox. All CD data were collected on a J-810 spectropolarimeter (Jasco).

EPR Spectroscopy. The four-Fe cluster in IspH can be reduced by the addition of dithionite. Incubation with both dithionite and the substrate HMBPP does not result in the detection of an intermediate signal under the conditions used. An “intermediate signal” was induced by incubating the enzyme with an excess of dithionite and subsequently removing the excess by running the sample over a desalting PD10 column. The cluster remains reduced after this procedure, and this represents the “one-electron-reduced” form of the enzyme. Addition of HMBPP to this form induced the disappearance of the cluster signal and the formation of a new EPR signal, which for the sake of convenience is called FeS_A .

Continuous wave (CW) EPR spectra were recorded at X-band (9 GHz) frequency on a Bruker EMX spectrometer, fit with the ER-4119-HS high-sensitivity perpendicular-mode cavity. General EPR conditions were as follows: microwave frequency, 9.385 GHz; field modulation frequency, 100 kHz; field modulation amplitude, 0.6 mT. Sample specific conditions are given in the figure legends. The Oxford Instrument ESR 900 flow cryostat in combination with the ITC4 temperature controller was used for measurements in the 4–300 K range using a helium flow. Measurements at 77 K were performed by fitting the cavity with a liquid nitrogen finger Dewar.

A copper perchlorate standard (10 mM CuSO_4 , 2 mM NaClO_4 , and 10 mM HCl) was used for spin quantifications on spectra measured under nonsaturating conditions by comparison of the double integral of the signal from the samples with that from the standard. Signal intensities are presented as the amount of spin, which is the fraction of the amount of the EPR signal detected over the amount of $[\text{4Fe-4S}]$ cluster present in the sample.

Pulsed EPR and ENDOR data (35 GHz and 2 K) were obtained with an instrument described previously.^{42,43}

RESULTS

Relationship between Cluster Type and Enzyme Activity. The purified *A. aeolicus* enzyme shows the typical 420 nm band characteristic of cuboidal iron–sulfur cluster-containing proteins (Figure 3, black line). There is a small

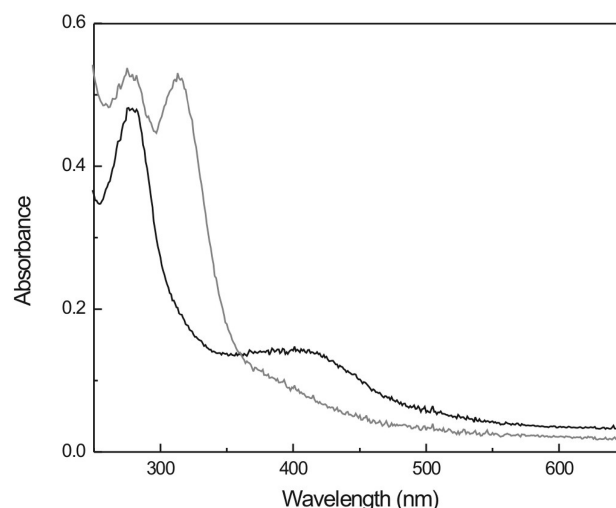


Figure 3. UV–visible absorption of as-isolated (black) and dithionite-reduced (gray) IspH protein from *A. aeolicus*. The peak at 330 nm is due to dithionite.

shoulder at 320 nm that can be assigned to bound single-iron ions (see below). The 420 nm band can be due to $[\text{4Fe-4S}]^{2+}$ clusters, $[\text{3Fe-4S}]^+$ clusters, or a mixture of both. Typically, these clusters can be reduced to the $[\text{4Fe-4S}]^+$ or $[\text{3Fe-4S}]^0$ forms by dithionite. This is also the case here, as detected by the bleaching of the 420 nm band upon addition of dithionite (Figure 3, gray line). The increase in absorbance at around 330 nm is due to dithionite. Similar spectra of as-isolated and reduced proteins were obtained for the WT enzyme from *E. coli* and *P. falciparum* (Figures S1 and S2 of the Supporting Information).

Comparison of the as-isolated and dithionite-reduced IspH enzymes in EPR spectroscopy shows that only for the *A. aeolicus* enzyme was an EPR signal from a $[\text{3Fe-4S}]^+$ cluster detected (Figure S3 of the Supporting Information, trace A). That signal, however, represents <1% of the total cluster content. The *P. falciparum* and *E. coli* enzymes do not show three-Fe cluster signals in the as-isolated forms (not shown). Instead, Figure 4 shows strong $[\text{4Fe-4S}]^+$ signals from the IspH enzymes of the three different organisms. The data thus show that the main cluster type present in all three enzymes is the four-Fe cluster. The three-Fe cluster content in IspH from all three sources can be increased by exposing any of these enzymes to air (not shown). The three-Fe clusters, however, do not accumulate to significant levels but are intermediate forms on the way to complete cluster breakdown.

Figure 5 shows the relationship between cluster content and enzymatic activity for IspH from *P. falciparum*. This enzyme was chosen because it displayed the highest (reconstituted) cluster content of all three IspH enzymes studied. Different samples were prepared for this plot. The first type was as-isolated enzyme ($\pm 15\%$ cluster content), the second type enzyme that was reconstituted (60 or 86% cluster content), and the third type enzyme that was exposed to air for a prolonged period of time (0% cluster content). All types were run over a 5

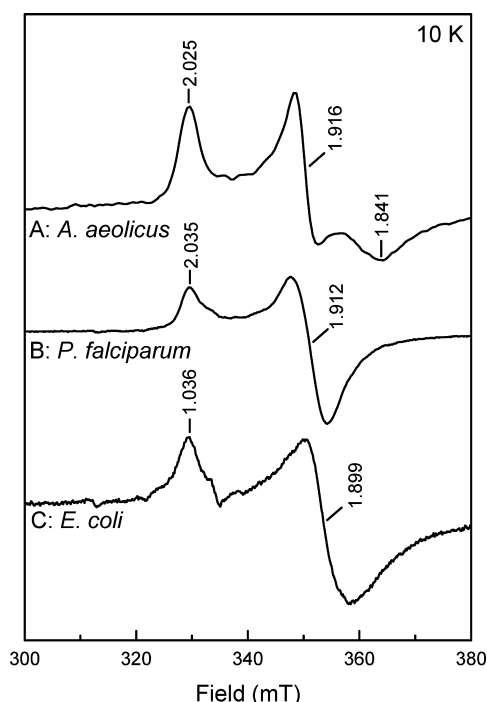


Figure 4. EPR spectra of the $[4\text{Fe-4S}]^+$ cluster in IspH protein from *A. aeolicus* (A), *P. falciparum* (B), and *E. coli* (C). The signal intensities have been adjusted for easy comparison. Microwave power of 0.2 mW.

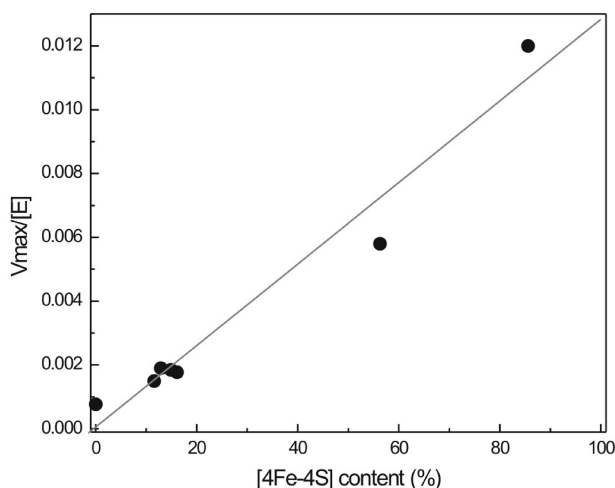


Figure 5. Relationship between enzyme activity and $[4\text{Fe-4S}]$ cluster content for *P. falciparum* IspH. The cluster content was calculated from the protein iron content.

mL column containing Chelex 100 resin to remove nonbound and adventitiously bound iron. In the case of the WT enzyme, the 420 nm band is not affected to a great extent by the Chelex treatment, but the shoulder at 320 nm is (Figure S4 of the Supporting Information). Therefore, this band is assigned to single-iron ions coordinated to one or more of the Cys residues present in the active site. The cluster content was determined after the Chelex treatment. Control EPR measurements showed that either no or very low-intensity three-Fe cluster signals were present in the samples, confirming that all clusters that are present have the four-Fe form. The cluster content was calculated on the basis of the determination of the iron content. Figure 5 shows that there is a linear relationship between $[4\text{Fe-4S}]$

cluster content (plotted as a percentage) and enzyme activity (plotted as $V_{\text{max}}/[E]$).

For the sake of completeness, it must be noted that the EPR spectrum of the dithionite-reduced *A. aeolicus* enzyme shows a feature, at around 100–150 mT, that can be attributed to a form of the $[4\text{Fe-4S}]^+$ species with an $S = 3/2$ spin, in addition to the signal from a form with an $S = 1/2$ spin between 300 and 350 mT⁴⁴ (Figure S3 of the Supporting Information, trace B). Addition of ethylene glycol enhances the $S = 1/2$ spin contribution and sharpens its EPR signal to one with g_1 , g_2 , and g_3 values of 2.035, 1.916, and 1.841, respectively (Figure S3 of the Supporting Information, trace C, and Figure 4, trace A).

Detection and Characterization of Reaction Intermediates for the WT Enzyme. On the basis of the fact that the $[4\text{Fe-4S}]$ cluster can donate only one electron at a time and the reaction requires two electrons, it could be expected that there would be a short-lived one-electron-reduced HMBPP species during the reaction. The incubation of the reduced enzyme in the presence of excess HMBPP and excess dithionite resulted in the disappearance of the $[4\text{Fe-4S}]^+$ signal (Figure S5 of the Supporting Information, traces A and B), indicating that the enzyme was being oxidized by the addition of substrate. No other signals were detected, however, within a time interval of 6 s to 5 min (not shown). This indicates that under normal steady-state conditions no intermediate accumulates to any high extent.

Next we investigated what would happen if only one electron was available for the reaction. One-electron-reduced protein can be obtained by incubating IspH with dithionite and removing the excess dithionite anaerobically with a PD10 desalting column. Optical spectroscopy (Figure S6 of the Supporting Information, dashed trace) shows that after this treatment the cluster stays reduced because the 420 nm band is still absent and nearly all dithionite has been removed because only a small band is still present at 330 nm. (This band can be completely removed when the procedure is repeated.) The cluster was still present as $[4\text{Fe-4S}]^+$ as shown by EPR spectroscopy (Figure S5 of the Supporting Information, trace C). The incubation of the one-electron-reduced *A. aeolicus* protein with HMBPP resulted in the formation of a new paramagnetic species (Figure 6, trace A, black line, and Figure S5 of the Supporting Information, trace D). This species is not an isolated organic radical, indicated by the large spread in g values: g_1 , g_2 , and g_3 values of 2.173, 2.013, and 1.997, respectively. EPR samples that were made with ^{57}Fe -enriched WT *A. aeolicus* IspH showed a significant broadening of the EPR signal (Figure 6, trace A, gray line). The broadening from the nuclear spin of ^{57}Fe shows that the signal is iron–sulfur cluster-based. For the discussion here, we will call this signal FeS_A . For the sake of completeness, the experiments with one-electron-reduced enzyme were performed for the *E. coli* and *P. falciparum* enzymes. In both cases, a new EPR signal was detected with properties almost identical to those of *A. aeolicus* enzyme (Figure 6, traces B and C). When additional dithionite was added to one-electron reduced IspH incubated with HMBPP, the FeS_A signal disappeared, again showing it is probably not a dead-end product.

It was noted that several of the samples contained an additional EPR signal due to Mn^{2+} ions. In a study by Rohdich and co-workers, it was found that the activity of the IspH enzyme in *E. coli* cell extracts was significantly higher in the presence of divalent metal ions like Co^{2+} and Mn^{2+} .⁴⁵ None of the crystal structures, however, showed the presence of

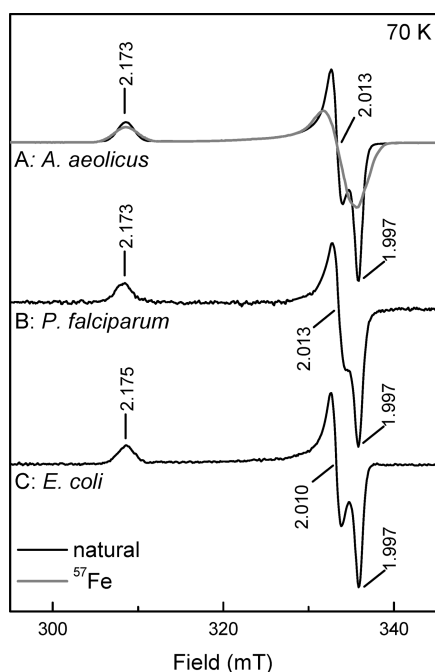


Figure 6. EPR signals of the FeS_A species detected in IspH from *A. aeolicus* (A), *P. falciparum* (B), and *E. coli* (C). The spectra for the *A. aeolicus* IspH are for enzyme from cells grown on natural abundance iron-containing medium (black) and cells grown on ⁵⁷Fe-enriched medium (gray). Microwave power of 2 mW.

additional metal ions. The spectroscopic behavior of all three enzymes in our studies was identical regardless of whether the Mn²⁺ signal was present, suggesting that this ion does not play a direct role in catalysis.

For the sake of completeness, the temperature dependence of the EPR signals and their amplitudes were measured for both the [4Fe-4S]⁺ and FeS_A species. The [4Fe-4S]⁺ state shows representative behavior for such a cluster: above 20 K, the signal becomes broader (Figure S7A of the Supporting Information). Conversely, the FeS_A signal can be observed up to 75 K without shifts or extensive broadening (Figure S7A of the Supporting Information).

Figure 7 shows 35 GHz CW EPR and ³¹P-Mims ENDOR spectra for FeS_A prepared from *P. falciparum* IspH and HMBPP. The ENDOR spectra show a doublet centered at the ³¹P Larmor frequency with a small, highly anisotropic hyperfine splitting with a maximal coupling (A_{max}) of 0.17 MHz. Simulations show that the maximal dipolar coupling is $2T_{\text{max}} \approx A_{\text{max}}$ with a negligible isotropic coupling (not shown). The observation of this signal indicates the presence of a substrate ³¹P nucleus in the proximity of the cluster spin, while the small coupling means that the phosphate group is not directly bound to the cluster. Detailed information about spin coupling within the cluster would permit a reliable estimate of the distance from ³¹P to the cluster. However, for heuristic purposes, we may assume the cluster to act as a point spin on a single nearby Fe ion of the FeS cluster ($2T_{\text{max}} \sim 2g\beta_n\beta_n/r^3 = 0.17$ MHz), which gives a representative Fe–³¹P distance (r) of ~ 7 Å.

Figure 8 shows two-dimensional (2D) field-frequency ²H ENDOR spectra comprised of spectra collected across the EPR envelope of FeS_A prepared by incubating the reduced enzyme with HMBPP labeled with deuterium at the C4 position. The labeled compound was synthesized as a racemate mixture. From the perspective of an ENDOR measurement, an

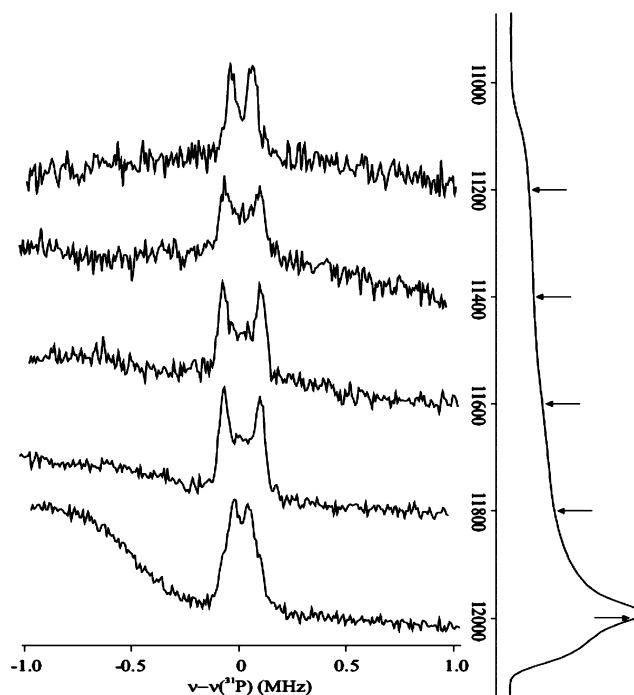


Figure 7. CW EPR (35 GHz) and pulsed ³¹P ENDOR spectra of the FeS_A species. Spectra were recorded at the positions indicated on the pulse echo-detected EPR spectra shown at the right. ENDOR spectra are normalized to a fixed intensity for the sake of clarity. The sample contained 1.7 mM one-electron-reduced IspH from *P. falciparum* and 33 mM HMBPP. The sample was incubated for 25 s at room temperature before being frozen. Conditions for the Mims pulse sequence: microwave pulse length, 30 ns; RF pulse length, 20 μs; repetition rate, 20 ms; τ , 800 ns; microwave frequency, 34.871 GHz; temperature, 2 K.

intermediate prepared with such a mixture is equivalent to a preparation with 50% of the dideutero compound and will be discussed as such. The spectra exhibit ν_+ / ν_- branches centered at the ²H Larmor frequency and separated by the ²H hyperfine coupling; each branch is further broadened and/or split by ²H quadrupole interactions. The hyperfine splitting is considerably anisotropic, with maximal coupling (A_{max}) of ~ 1.4 MHz at g_2 . The presence of two magnetically inequivalent deuterons whose hyperfine couplings may differ and whose hyperfine and quadrupole tensor orientations in general will differ leads to the broad and poorly defined ν_+ / ν_- branches except in the vicinity of g_3 , where the spectrum is most highly resolved. At g_3 , a set of four lines that almost certainly correspond to the quadrupole-split doublet of a single deuteron ²H₁ can be seen with an observed quadrupole coupling $3P$ of 0.13 MHz and a hyperfine coupling A of 0.54 MHz. Two weaker peaks observed in the g_3 spectrum are then assigned to ²H₂, with a smaller hyperfine coupling at g_3 .

Although ENDOR transitions arising from ²H₂ undoubtedly contribute across the entire pattern, the majority of the 2D pattern can be reasonably well described in terms of a dominant contribution from ²H₁. One begins by assigning A_{max} to ²H₁ and recognizing that the value of the quadrupole splitting for $3P(^2\text{H}_1)$ at g_3 suggests that this is likely to be associated with the “perpendicular” component ($3P_{\perp}$) of the axial C–H quadrupole interaction. A series of simulations (not shown) then allows an estimate of the hyperfine tensor components for ²H₁ ($A \sim [0.5, 1.4, 0.5]$ MHz) with an isotropic contribution of

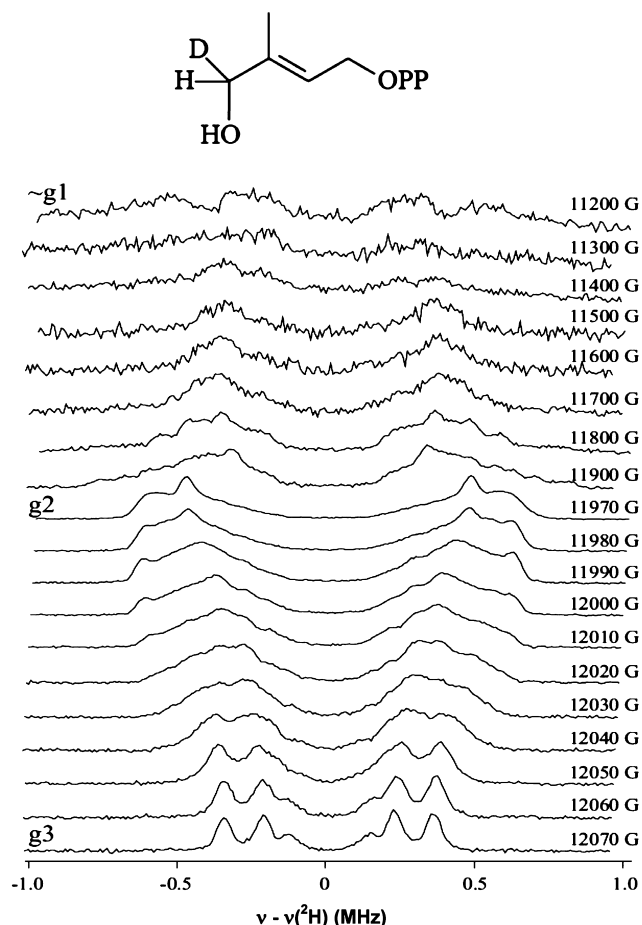


Figure 8. Pulsed ^2H ENDOR spectra of the FeS_A species. Spectra were recorded at the field positions indicated. The sample contained 1.2 mM one-electron-reduced IspH from *P. falciparum* and 33 mM $[\text{HMBPP}]^{2-}$. The sample was incubated for 25 s at room temperature before being frozen. Conditions for the Mims pulse sequence: microwave pulse length, 30 ns; RF pulse length, 20 μs ; repetition rate, 20 ms; τ , 800 ns; microwave frequency, 34.871 GHz; temperature, 2 K.

$a_{\text{iso}}(^2\text{H}_1)$ of ~ 0.8 MHz, corresponding to an $a_{\text{iso}}(^1\text{H}_1)$ of ~ 5 MHz. A heuristic distance calculation, similar to that performed for ^{31}P described above, furnishes an Fe–D distance to the deuterium of C4 of 3.4 Å, undoubtedly an underestimate because it ignores any local anisotropic contribution. The presence of such a large isotropic interaction requires that FeS_A contain HMBPP or a product of its reaction that is bound to the paramagnetic cluster. The size of a_{iso} further suggests that C4 is adjacent to the site coordinated to the metal ion, consistent with binding of the hydroxyl group to the unique Fe of the cluster, as seen in the *E. coli* crystal structure showing that substrate binds to the oxidized cluster.

To further explore binding of substrate to *A. aeolicus* IspH, we used CD spectroscopy. The oxidized cluster present in the reconstituted protein shows a broad feature only at ~ 350 nm (Figure S8 of the Supporting Information, black trace). The spectrum changes significantly in the presence of 1 equiv of HMBPP (Figure S8 of the Supporting Information, gray trace). Additional equivalents of HMBPP caused no further change. This finding is consistent with binding of the HMBPP hydroxyl to the $[\text{4Fe-4S}]^{2+}$ cluster. Analogous results were obtained by monitoring changes in the Mössbauer spectra of the $[\text{4Fe-4S}]^{2+}$ cluster induced by treatment with HMBPP.⁴⁶

Studies with Mutant IspH. On the basis of computer modeling studies with the *A. aeolicus* enzyme and the *E. coli* structure with bound HMBPP, residues His42, His124, and Glu126 (*A. aeolicus* numbering) are predicted to have important roles in the binding of HMBPP and/or the reaction itself. To test this, we introduced two mutations at each of the three positions, 42, 124, and 126: H42A and H42F, H124A and H124F, and E126A and E126Q.

All IspH mutants were expressed at similar levels as seen for WT IspH. CD spectra measured for WT and mutant proteins all are very similar, indicating that the proteins are folded properly (Figure S9 of the Supporting Information). Absorption spectroscopy (not shown) showed that all mutants contained four-Fe clusters. The cluster content was in the range of 10–20%. Several of the mutants also displayed a more intense 320 nm band in absorption spectroscopy due to bound iron. Running the samples over a Chelex column greatly reduced the intensity of the 320 nm band (not shown). The cluster content could be increased to 40 to 50% for the different mutants by the cluster reconstitution procedure (Table 1).

Table 1. Comparison of the Properties of WT and Mutant *A. aeolicus* IspH

reconstituted enzyme	cluster content (%)	specific activity after correction for cluster content ($\mu\text{mol min}^{-1} \text{mg}^{-1}$)	K_M (μM)	k_{cat}/K_M
WT	42.9	1.95	6.4	0.30
H42A	29.9	0.20	1.7	0.12
H42F	45.9	1.09	144	0.008
H124A	33.2	0.14	1.2	0.12
H124F	35.6	0.20	33.6	0.006
E126A	41	0.19	2.4	0.08
E126Q	29.6	0.20	0.4	0.50

Activity assays were performed for all six protein variants, as well as the wild-type enzyme (Table 1). The values in Table 1 are similar to those reported in the literature.³² Comparison of the specific activities shows that all mutants, except the H42F mutant, have greatly diminished activity in the range of 5–10% of that of the WT enzyme. H42F has $\sim 50\%$ of the WT activity remaining. Because of the low activity present in most of the mutants, it was difficult to obtain the data, and small changes in K_M and catalytic efficiency should not be overinterpreted. A clear difference in catalytic efficiency, however, is found for the H42F and H124F mutants. The Phe residue in the H42F mutant seems to be able to rescue the loss of activity observed in the H42A mutant, but at the same time, the K_M value increases to 144 μM , causing a large decrease in the catalytic efficiency. A similar effect is found for the H124F mutant. This indicates that the N atoms in the His imidazole ring play an important role in the binding of HMBPP.

EPR spectra collected from as-isolated and cluster-reconstituted mutant proteins are equivalent, except that signal-to-noise ratios were much better in the reconstituted enzyme. Representative samples of each type were used to make the figures. As-isolated mutated proteins show at most only small amounts of the $[\text{3Fe-4S}]^+$ cluster; WT and H42A show only radical-type species of unknown origin, not three-Fe clusters (Figure S10A of the Supporting Information). After addition of dithionite to the mutant proteins, the $[\text{4Fe-4S}]^+$ cluster EPR signal was detected in all mutants (Figure S10B of the Supporting Information), with an intensity much higher than the intensity of the $[\text{3Fe-4S}]$ signals (if any). Hence, we can

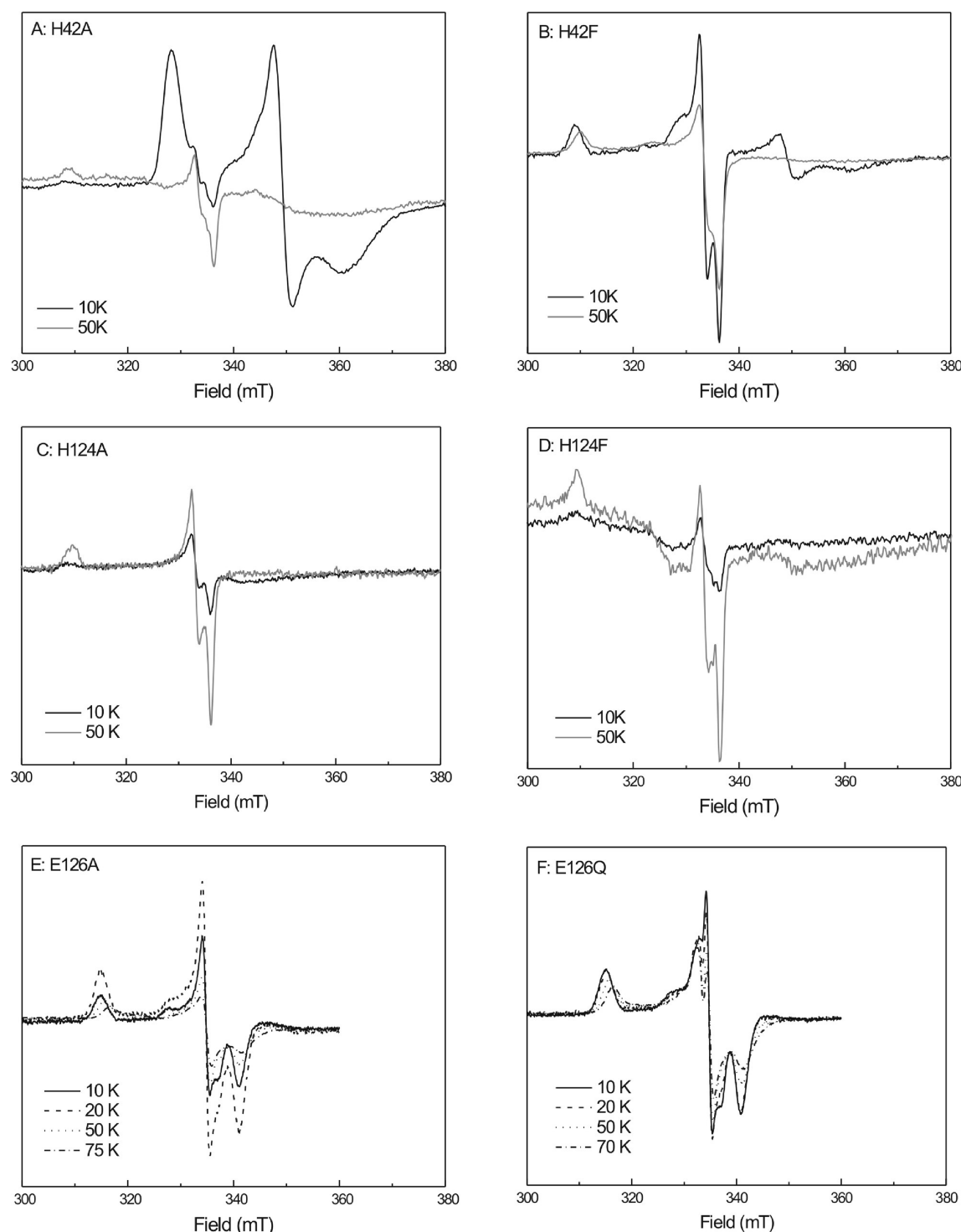


Figure 9. Temperature behavior studies of FeS_A with reconstituted mutant enzymes from *A. aeolicus*. Spectra are presented as an overlay using normalized spectra. All spectra are corrected for differences in gain, temperature, and power: (A, D, and E) data for the as-isolated enzyme and (B, C, and F) data for the reconstituted enzyme.

conclude that for mutants the main cluster type present again is the $[\text{4Fe-4S}]$ cluster, and the similar g values show the clusters are no more than minimally perturbed. However, small differences with the WT enzyme can be observed upon addition of 20% EG. This results in different ratios of $S = 1/2$ and $S = 3/2$ species for the different mutants. In the case of the Glu126 mutants, no conversion to the $S = 1/2$ form was

observed. When 33–40% EG was added, however, all mutants showed some $S = 1/2$ signal in the $g = 2$ region (not shown).

When one-electron-reduced mutant enzymes were prepared and incubated with HMBPP, several new signals were detected (Figure 9). Some were similar to those of the WT FeS_A species, but differences in temperature behavior were seen. Consider first the H42 mutants. Figure 9A shows the temperature variation of spectra from the H42A mutant. At 10–20 K, an

EPR signal due to the $[4\text{Fe-4S}]^+$ cluster can be detected. At higher temperatures, the FeS_A species can be detected but the signal intensity is very low (0.03 spin). As this mutant has low activity, we can conclude that not much reaction is taking place. Different results were obtained for the H42F mutant (Figure 9B). At lower temperatures (from 5 to 20 K), a mixture of the $[4\text{Fe-4S}]^+$ signal and the FeS_A signal is present. At 50 K, only the FeS_A signal can be detected. Whereas the H42A mutant shows low activity and its four-Fe cluster remains reduced upon addition of HMBPP, when HMBPP is added to the H42F mutant a partial oxidation of the four-Fe cluster was detected and the FeS_A species was formed. This is in line with the activity data that show that this mutant is still active, although lower activity is observed. When the temperature is increased from 50 to 70 K, the intensity of the H42F- FeS_A signal decreases because of relaxation broadening. This differs from the very wide temperature range over which the WT- FeS_A signal can be detected.

Next consider the H124 mutants. Neither the H124A mutant nor the H124F mutant shows significant activity (Table 1), so it might be expected that they would show the same behavior as the H42 mutants. This is not true, however. Addition of substrate to the H124A or H124F mutant causes the loss of the EPR signal because of the $[4\text{Fe-4S}]^+$ cluster (Figure 9C), which indicates that the cluster becomes oxidized upon addition of substrate. This oxidation, however, is accompanied by the formation of only very low levels of the FeS_A species (<0.01 spin). The FeS_A species found in these mutants also showed temperature broadening at 70 K, unlike the WT signal.

There could be several reasons that the cluster in the H124A and -F mutants seems to become oxidized, with the formation of little or no FeS_A . In some samples, other radical-like signals were observed with g_1 , g_2 , and g_3 values of 2.041, 2.034, and 2.015, respectively (Figure 10A). This suggests that the binding of HMBPP is affected in such a way that electron transfer results in an alternative radical species that is not stabilized by interaction with the cluster. Several samples also showed broad EPR signals (Figure 10B). From the g values, we can conclude that the signal is due to a paramagnet with an $S = 3/2$ spin. This signal is different from that detected in the reduced enzyme (see Figure 4 and Figure S3 of the Supporting Information). The H124 spectra have $g = 4.69$ and 3.33 peaks that correspond to an E/D value of 0.11. Because the latter signal is detected in the presence of HMBPP, it could also be due to a cluster-HMBPP complex. The binding, however, appears to be unproductive, not resulting in the formation of the FeS_A species.

Finally, consider the E126A and -Q variants (Figure 9E,F). When the two one-electron-reduced enzymes are treated with substrate, both show a signal, with g_1 , g_2 , and g_3 values of 2.120, 2.002, and 1.965, respectively. These values are identical to those for the species described by Wang et al.³² The signal remains sharp up to 10 and 20 K but becomes broader at higher temperatures. Studies with excess dithionite (not shown) showed that this species, in opposition to the FeS_A -like species detected in the other mutants, is not an intermediate whose signal is lost upon further reaction but accumulated over time. The E126Q mutant also shows an additional species at ~332 mT. It was not possible to obtain a clean EPR signal for this species by subtraction because the main species in these samples showed additional temperature broadening in each spectrum, which induced additional features in the difference spectra.

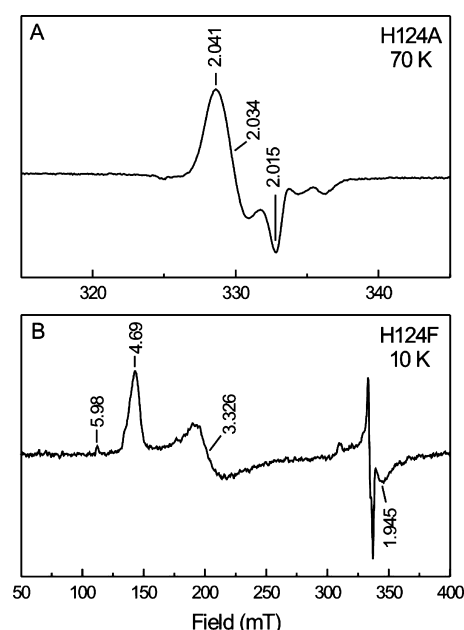


Figure 10. Additional paramagnetic species detected in some of the mutant IspH enzymes from *A. aeolicus*. (A) Possible organic radical observed in one-electron-reduced H124A IspH after addition of HMBPP and incubation for 20 s. (B) $S = 3/2$ EPR signal observed in one-electron-reduced H124F IspH after addition of HMBPP and incubation for 20 s. The signal in the 300–350 mT region is the FeS_A EPR signal.

DISCUSSION

In this paper, we have shown that the active form of the IspH enzyme contains a $[4\text{Fe-4S}]$ cluster. The EPR signal of this cluster disappears when the enzyme undergoes catalytic turnover with the substrate HMBPP in the presence of excess dithionite, and no new EPR signals appear. The conversion of HMBPP into IPP or DMAPP requires two electrons. Therefore, the one-electron-reduced form of the enzyme was prepared with the aim of trapping a reaction intermediate. This strategy was successful, and incubation of the reduced enzyme with HMBPP resulted in the disappearance of the $[4\text{Fe-4S}]^+$ signal and the appearance of a new signal. Labeling studies with the ^{57}Fe isotope showed that the signal is associated with the $[4\text{Fe-4S}]$ cluster, so it was dubbed FeS_A . The EPR properties of the FeS_A signal, in particular its temperature response, are very different from those of regular four-Fe clusters of proteins involved in electron transport.⁴⁷ They are, however, very similar to those of intermediates detected in two other $[4\text{Fe-4S}]$ cluster-containing enzymes, (E)-4-hydroxy-3-methylbut-2-enyl diphosphate synthase (IspG/GcpE), the penultimate enzyme in the DOXP/MEP pathway, and ferredoxin:thioredoxin reductase (FTR), an enzyme present in oxygenic photosynthetic organisms.^{48–52} In those two cases, there is evidence that the reaction mechanisms involve the attachment of a substrate (IspG) or an additional amino acid (FTR) to the four-Fe cluster. In the recently proposed IspH mechanism I,^{32,33} HMBPP first coordinates to the cluster through the oxygen of the hydroxyl group at C4 (Figure 1). Subsequent electron transfer results in the formation of a π (or π/σ) complex. Before the properties of the cluster-bound reaction intermediate are discussed in more detail, a discussion of the mutagenesis studies is important because the model in Figure 1

is based on a signal detected in the E126A mutant that differs from the FeS_A signal detected in WT IspH.

IspH Mutants. Examination of the crystal structures of IspH protein from *A. aeolicus* and *E. coli* mutants led to the construction of pairs of mutants at three sites: H42A and H42F, H124A and H124F, and E126A and E126Q. Absorption, CD, and EPR measurements show that the mutant enzymes are properly folded and contain four-Fe clusters. As the cluster content was low, reconstitution of the clusters was performed. Analysis of the enzymatic activity of the mutants thus prepared showed that only the H42F mutant shows relatively high activity (Table 1).

His42 was chosen as a mutation site because it was proposed to participate in the interaction with one of the diphosphate oxygens of HMBPP. Replacement of His42 with Ala caused a 90% decrease in activity. The incubation of one-electron-reduced H42A with substrate does not result in oxidation of the four-Fe cluster or the formation of the FeS_A species in significant amounts. The mutation of His42 into Phe resulted in an enzyme that still showed partial activity and formed the FeS_A species. The observed V_{max} is approximately half of that of the WT enzyme at comparable cluster occupancies. Because the His42 residue is too far from the HMBPP hydroxyl group to be directly involved in the reaction and is not involved in coordination of one of the “conserved” water molecules detected in the crystal structures, the mutation must have an effect on the binding of substrate and/or the conformation of the active site. Having a Phe residue at this position instead of an Ala residue appears to rescue some of the activity. The loss of activity could have been due to a structural effect, and with a Phe instead of an Ala, the local conformation is less perturbed by the conservation of the ring structure. At the same time, however, the absence of the N atoms causes a large increase in K_M and a large decrease in catalytic efficiency. This confirms the role of H42 in binding of HMBPP.

His124 was proposed to participate in the interaction with one of the diphosphate oxygens of HMBPP. Both His124 mutants show the loss of the $[\text{4Fe-4S}]^+$ signal upon addition of HMBPP but hardly any formation of the FeS_A signal. In some samples, an additional paramagnetic species was detected (Figure 10, trace A). The g values of this species (g_1 , g_2 , and g_3 values of 2.041, 2.034, and 2.015, respectively) are more in line with a carbon-based radical species. At the same time, some of the samples show a new $S = 3/2$ signal upon addition of HMBPP (Figure 10, trace B). The best way to interpret the data is to assume that an alternative cluster–HMBPP complex is formed or that HMBPP binds to the active site in the proximity of the cluster. In both cases, the position of HMBPP is such that the transfer of an electron to HMBPP still takes place but that upon transfer a free-standing radical species is formed instead of the FeS_A species. As a result, the enzyme becomes mostly inactive. Thus, the His124 residue is indeed important for HMBPP binding, in particular for the correct orientation of HMBPP in the active site. This result also gives a possible lead in finding inhibitors for this enzyme. Any HMBPP analogues that cause formation of the radical instead of formation of the FeS_A species could potentially knock out the enzyme and block the MEP/DOXP pathway.

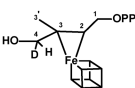
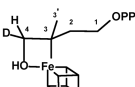
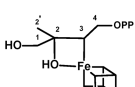
Glu126 was proposed to participate in acid–base chemistry at the active site and to have an important function in the reaction mechanism, either directly or through a hydrogen-bonded water molecule. The low activity of the Glu126 mutants supports this proposal. Upon addition of HMBPP to

both E126A and E126Q, the $[\text{4Fe-4S}]^+$ signal disappears and a new paramagnetic species is formed that is different from FeS_A detected in the WT and the other IspH mutants. Its EPR signal is identical to that detected for the E126Q species in previous work by Wang et al.³² A further discussion of this species is presented below.

In summary, the mutagenesis data support the proposed roles of the three residues, His42, His124, and Glu126, in the binding and positioning of the substrate and in catalysis. In all cases studied here, addition of substrate to the mutant enzyme with a reduced cluster caused the loss of the cluster signal, demonstrating the interaction between the substrate and cluster in the presence of the mutations. This is the first time that these effects are described in detail.^{29,32} The crystal structures of IspH show that there is an extensive hydrogen bond network among the enzyme, HMBPP, and several water molecules that are present in most of the structures.²⁹ In particular, the HMBPP diphosphate group in IspH from *E. coli* is bonded by seven amino acid residues: H74, H41, S269, S225, N227, S226, and H124. The H41Q and H74Q mutants were still active;²⁹ the H124N, S225C, and N227Q mutants were not,²⁹ while the H41A, H74A, and H124A mutants afforded insoluble protein.²⁹ With so many hydrogen bonds available, a single mutation might not be expected to have a severe effect on the binding of HMBPP. Instead, however, some of the mutants show very low levels of activity or the inability to fold properly, indicating the importance of these few residues in maintaining the local protein structure. Previous studies did not allow a conclusion about whether the loss of activity in properly folded mutants is due to weakened binding of HMBPP or changes to the active-site structure. These studies of the spectroscopic properties of the mutant enzyme and in particular the $[\text{4Fe-4S}]$ cluster provide a more in-depth understanding of the role of (mutated) amino acid residues His42, His124, and Glu126.

Mechanistic Implications. The paramagnetic center detected in the catalytically inactive E126Q mutant incubated with dithionite and HMBPP was the first possible intermediate state of IspH to be fully characterized by EPR and ENDOR spectroscopy.^{32,53} ^{13}C ENDOR studies of the E126Q species incubated with $[\text{U-}^{13}\text{C}]\text{HMBPP}$ showed the presence of two pairs of peaks that were attributed to two different carbon atoms with couplings of 1.7 and 0.8 MHz (Table 2). On the basis of an analogy to the bio-organometallic center characterized during reduction of alkynes by nitrogenase,⁵⁴ a side-on binding of the double bond of HMBPP to the unique iron in IspH was proposed. Although the coupling values are relatively large, larger ^{13}C couplings have been found for substrates where the ^{13}C is not bound to the metal ion, for example, in the formaldehyde-inhibited form of the molybdoenzyme, xanthine oxidase,⁵⁵ where a ^{13}C coupling $a_{\text{iso}}(^{13}\text{C})$ of 43 MHz was determined for a ^{13}C derived from formaldehyde that is not directly bonded to the metal ion. Thus, a more in-depth, joint analysis of the ^{13}C and ^2H ENDOR would be welcome confirmation. Acetylenic diphosphate compounds, however, were shown to be very strong inhibitors of IspH. But-3-ynyl diphosphate, for example, has an IC_{50} of 0.45 μM . Consistent with the proposed structure for the HMBPP product, these were proposed to bind side-on. Hypothetical IspH mechanism II that is based on this side-on binding model is shown in Figure 11. It was proposed that the initial interaction of HMBPP with the cluster occurs via the oxygen of the hydroxyl group at C4. Subsequent electron transfer from an outside electron donor results in the formation of a π complex.

Table 2. Comparison of the Coupling Constants of Selected Atoms for the Different Proposed Reaction Intermediates^a

IspH E126Q ('species X')	Atom	a_{iso} (MHz)	ref
	D4	0.4	32
	¹³ C2,3	1.7 and 0.8	32
	³¹ P	<0.1	32
IspH WT-FeS _A			
	H4 (D4)	5.2 (0.8)	This study
	³¹ P	0.17	This study
IspG WT-FeS _A			
	H2'(D2')	12 (1.8)	33, 58, 61
	¹³ C2	17.7	33, 61
	¹³ C3	3.0	33, 61
	¹⁷ O	n.d.	33, 61

^aNot determined.

Deoxygenation of the substrate generates a water molecule and an η^1 -allyl complex by protonation (via Glu126) to the reduced complex. The second electron transfer yields an η^3 -allyl complex.

Here we describe the formation of the FeS_A species in the one-electron-reduced catalytically active enzyme upon incubation with HMBPP. The ENDOR data presented for FeS_A show a weak coupling from ³¹P of the diphosphate group, with a maximum of 0.17 MHz (Table 2). An approximate point dipole calculation gave an effective distance between the FeS cluster and the ³¹P of ~7 Å. The lack of any significant isotropic contribution and the large distance indicate that the phosphate

group is in the vicinity of the cluster, but not directly bound to it.

The ENDOR studies using HMBPP labeled with deuterium at C4 show the presence of ²H peaks corresponding to the two deuterium positions of the racemate mixture. Simulations give an excellent estimate for the hyperfine tensor of the more strongly coupled deuterium, assuming that it is H₁. The isotropic ²H₁ coupling is equivalent to a ¹H₁ coupling (a_{iso}) of 5.2 MHz and an effective H₁-cluster distance of ~3.4 Å, indicative that C4 is adjacent to the site of linkage between the FeS cluster and HMBPP, or its reaction product (Table 2). It is not possible to determine the precise hyperfine and quadrupole interaction tensors for the second deuterium. However, all these findings are consistent with an HMBPP bound to the cluster not through phosphate, but via attachment through the hydroxyl group or as a π complex.

How can we explain the differences between the FeS_A species and the species detected in the E126Q mutant, considering both the different g values and the observed coupling constants (Table 2)? It is possible that both represent a reaction intermediate at different points in the reaction cycle. Given that the Glu126 mutation is catalytically inactive, it is also possible, however, that the Glu126 mutation resulted in the formation of a dead-end product not directly related to the reaction mechanism. More studies are needed to discern between these two options.

Where would we place the FeS_A species in IspH mechanism II (Figure 11)? It might be just the complex formed by binding the hydroxyl of HMBPP to the reduced four-Fe cluster. However, with all the ingredients present for the conversion of HMBPP, there is no obvious reason why the reaction would not proceed from there all the way to the η^1 complex. This complex, however, is not paramagnetic and therefore cannot be the FeS_A species. This puzzle, along with the finding that the E126Q mutant is not active and that the putative side-on bound state might not represent a catalytic intermediate, leads us to next explore other mechanistic models.

Alternative Models. As mentioned earlier, there are two other enzymes that show EPR signals from catalytic

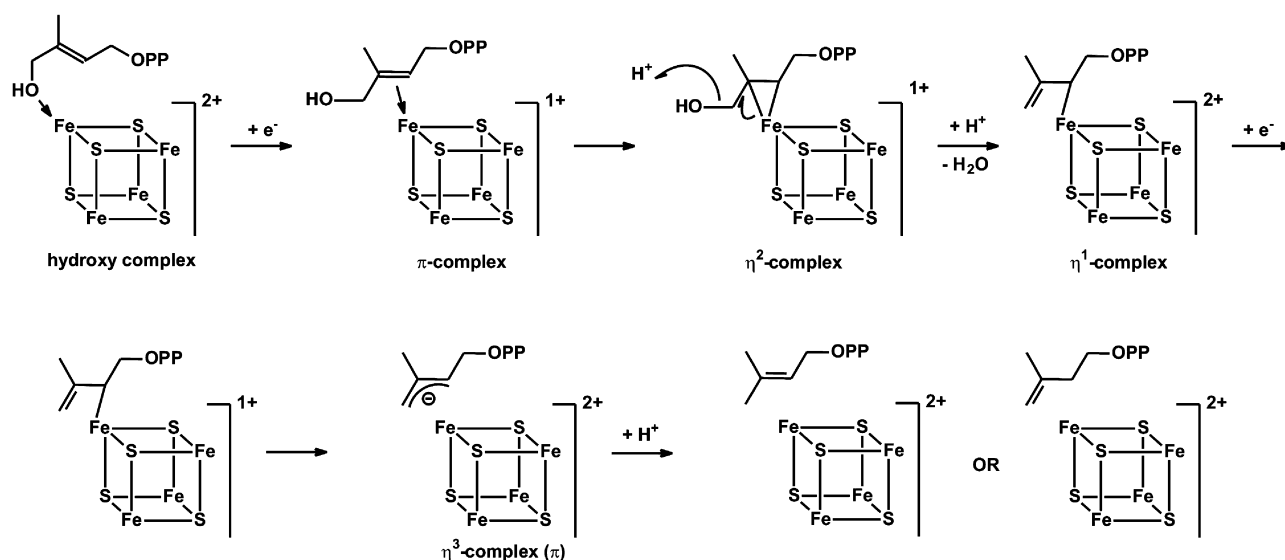


Figure 11. IspH mechanism II. Hypothetical reaction mechanism II for the conversion of HMBPP by IspH. Adapted from ref 32. See the text for details.

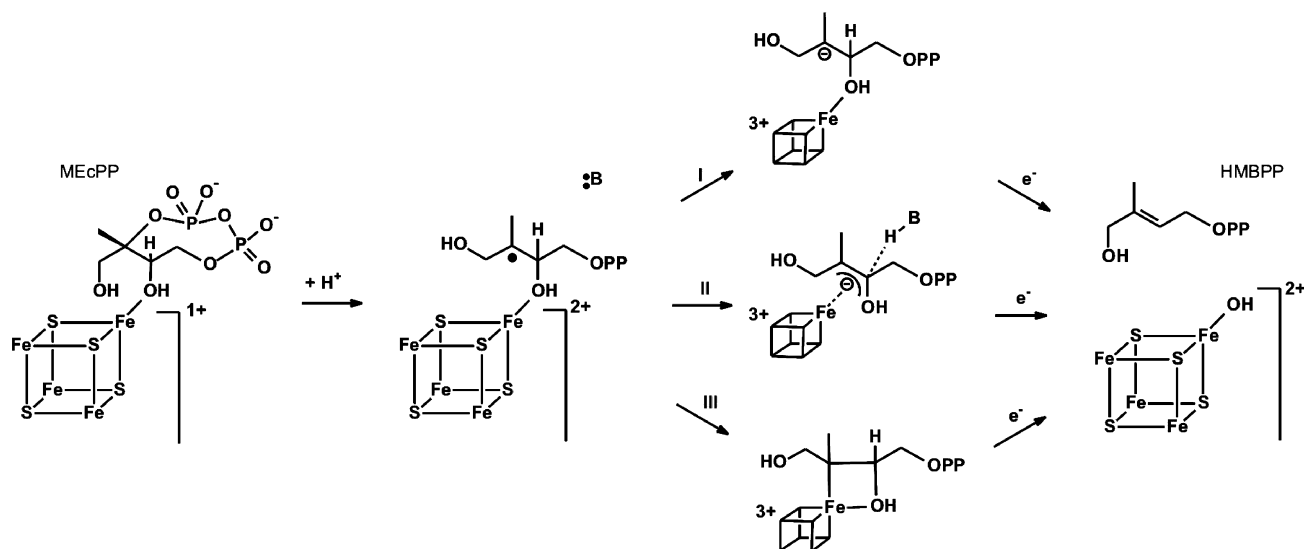


Figure 12. IspG mechanism I. Hypothetical reaction mechanism for the conversion of MEcPP by IspG. See the text for details.

intermediates that are very similar to the FeS_A signal observed in WT IspH. The first enzyme is FTR. This enzyme functions as a one-electron–two-electron switch, using single electrons donated by ferredoxin for a two-electron reduction of a disulfide bond present on the substrate enzyme thioredoxin. The active site of FTR contains the unique combination of a $[4\text{Fe-4S}]$ cluster in the proximity of an active-site disulfide.⁵⁶ The transfer of the first electron from the $[4\text{Fe-4S}]^+$ cluster to the disulfide would theoretically cause the formation of a thiolate and a thiyl radical. The formation of the radical species, however, is prevented by the formation of a bond between this sulfur atom and an iron atom of the four-Fe cluster.^{48,49,57} The unique iron site ends up being coordinated by two cysteines. This species is best described as a $[4\text{Fe-4S}]^{3+}$ cluster. The other enzyme is IspG. This enzyme is the penultimate enzyme in the MEP/DOXP pathway and converts 2-C-methyl-D-erythritol-2,4-cyclodiphosphate (MEcPP) into HMBPP (Figure 12). MEcPP is a cyclic compound, and the reaction involves the opening of the ring and removal of the C3 hydroxyl group consuming the total of two electrons. The enzyme contains a single $[4\text{Fe-4S}]$ cluster in its active site.

In a recent study of IspG,⁵⁸ we showed that several paramagnetic species could be observed in steady-state and pre-steady-state kinetic experiments. One of these signals was from a transient species that was dubbed FeS_A , which displayed a rhombic EPR signal with g_1 , g_2 , and g_3 values of 2.087, 2.019, and 2.000, respectively. It is because the g values for FeS_A of IspH reported here are so similar to those for IspG (2.173, 2.013, and 1.997, respectively) that the signal induced in one-electron-reduced IspH incubated with HMBPP was also dubbed FeS_A . ^{31}P ENDOR measurements of the IspG– FeS_A species, like those of the IspH– FeS_A species, showed a weak ^{31}P coupling that is in line with binding of the substrate to the enzyme in the proximity of the active-site cluster.⁵⁸ On the basis of EPR and ENDOR measurements, it was proposed that the substrate binds directly to the $[4\text{Fe-4S}]$ cluster during the reaction. Parallel to this, labeling studies by Wang et al.³³ with the alternative substrate $[2,3-^{17}\text{O}]$ HMBPP epoxide showed that there is an Fe–O bond, in line with binding models for MEcPP via one of its hydroxyl groups or the formation of a more tightly bound ferraooxetane complex (Table 2). Thus, we inferred that

the iron–sulfur cluster is directly involved in a reductive elimination of a hydroxyl group in IspG, which thus suggests the same for IspH.

IspH and IspG catalyze a very similar reaction, the reductive elimination of a hydroxyl group. In both cases, a very similar paramagnetic species, thus denoted FeS_A , is formed during the reaction mechanism. We propose that in both enzymes the FeS_A species represents a reaction intermediate that is bound to the four-Fe cluster via a hydroxyl group. On the basis of the similarities with the EPR signal detected in FTR, we also propose that the FeS_A signals are due to an $[4\text{Fe-4S}]^{3+}$ species. This is supported by the fact that the FeS_A signals have an average g value that is greater than g_e , which is strongly indicative of a $[4\text{Fe-4S}]^{3+}$ species.^{59,60}

Key to proposing any reaction mechanism for IspH is the fact that a completely radical based mechanism should be avoided, because the carbon–oxygen bond connecting the diphosphate group to the rest of the molecule is more labile than the one connecting the hydroxyl group and would therefore have a higher chance of being broken in such a mechanism. IspH mechanism II (Figure 11) does avoid such a situation, but binding of the hydroxyl group to the cluster would make it a much better leaving group, favoring removal of the cluster-bound hydroxyl group. IspG mechanism I that we recently proposed is shown in Figure 12. In this case, the substrate MEcPP starts by binding to the cluster via the hydroxyl group that is ultimately eliminated. Protonation of MEcPP results in ring opening and the formation of a carbocation. The internal transfer of an electron from the cluster to the substrate results in the formation of a carbon radical. There are several possibilities of how the cluster can stabilize this radical species. One option would be the transfer of an additional electron, making the cluster formally $3+$ (reaction I). However, this would create a carbanion species that could be very reactive. The ferraooxetane structure as proposed by Wang et al.⁶¹ would provide a way to stabilize the carbanion (and even the radical species in the previous step) by forming an additional bond to the unique iron (via reaction III). At this point, it is not clear, however, if there is a direct bond between C3 and the unique iron. As an alternative (reaction II), a π/η -type complex can be proposed, perhaps accompanied by interaction with the hydroxyl oxygen. In either case, the transfer of the second

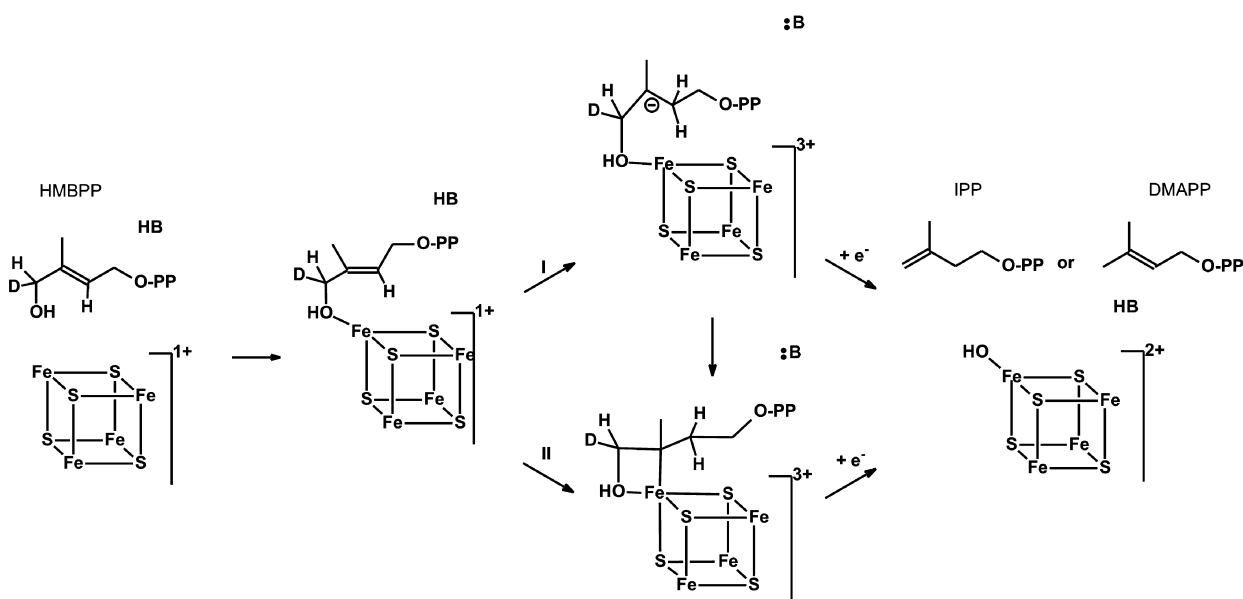


Figure 13. IspH mechanism III. Hypothetical reaction mechanism III for the conversion of HMBPP by IspH. See the text for details.

electron from the outside electron donor to the active-site cluster results in the release of the hydroxyl group and formation of a double bond. The hydroxyl group can stay bound to the cluster and comes off later because it is only weakly bound as shown, for example, for aconitase.⁶²

A similar approach is followed in IspH mechanism III (Figure 13). HMBPP can bind to either the $[4\text{Fe-4S}]^{2+}$ or $[4\text{Fe-4S}]^{1+}$ form of the enzyme. The transfer of two electrons from the cluster to the bound substrate results in the formation of a carbanion (reaction I). This could be stabilized by an additional interaction with the unique Fe of the cluster. In the most extreme case, there could be a direct bond between the iron and C3 (reaction II), similar to the ferraoxetane species proposed for IspG. Re-reduction of the cluster to the 2+ state by an outside electron donor causes the cleavage of the C–O(H) bond and the formation of either IPP or DMAPP.

IspH mechanism III (Figure 13) is a working model that includes the following assumptions: a direct Fe–O bond and a 3+ oxidation state for the cluster. These will be tested through a series of labeling studies with ^{13}C , ^{17}O , and ^{57}Fe , using a combination of ENDOR and Mössbauer spectroscopy. IspH mechanism III also does not explain why (*E*)-3-(fluoromethyl)-2-butenyl diphosphate (C4–F instead of C4–OH) is a substrate for this enzyme, as this compound has no hydroxyl group.³⁹ It is well-known that enzymes can employ different reaction mechanisms for substrates with different properties, and the possibility that this compound reacts via a different reaction mechanism will be tested via examination of the EPR signals induced by incubation of one-electron-reduced WT, E126A, or E126Q IspH with (*E*)-3-(fluoromethyl)-2-butenyl diphosphate.

Summary. This paper presents evidence of the important role of a $[4\text{Fe-4S}]$ cluster in the reaction mechanism of the IspH enzyme. The cluster is involved in direct binding of HMBPP that stays bound during the subsequent catalysis. A paramagnetic reaction intermediate, denoted FeS_A , is generated upon incubation of the one-electron-reduced enzyme with HMBPP, with EPR and ENDOR studies revealing that it contains an HMBPP-derived intermediate bound to the cluster. Similarities of this species with other paramagnetic inter-

mediates associated with $[4\text{Fe-4S}]$ cluster-containing enzymes, in particular a very similar species in the previous enzyme in the MEP/DOXP pathway, IspG, indicates an association via the C4 (hydroxyl) oxygen. Studies with the mutant enzyme confirmed the roles of His42 and His124 in binding of HMBPP and the role of Glu126 in the reaction mechanism. The role of His124 is particularly interesting because it appears to play a role in keeping the substrate HMBPP in the correct orientation so that the stable HMBPP–cluster complex can be formed. Mutating this residue resulted in the formation of a HMBPP-based radical instead.

■ ASSOCIATED CONTENT

§ Supporting Information

Additional EPR, electron absorption, and CD spectra for the three IspH proteins and the *A. aeolicus* mutants. This material is available free of charge via the Internet at <http://pubs.acs.org>.

■ AUTHOR INFORMATION

Corresponding Author

*Department of Chemistry and Biochemistry, Auburn University, Auburn, AL 36849. E-mail: duinedu@auburn.edu. Phone: (334) 844-6072.

Funding

This work was supported by National Science Foundation Grant 0848196 to E.C.D. and National Institutes of Health Grant HL 13531 to B.M.H.

Notes

The authors declare no competing financial interest.

■ ABBREVIATIONS

HMBPP, (*E*)-4-hydroxy-3-methylbut-2-enyl diphosphate; IPP, isopentenyl diphosphate; DMAPP, dimethylallyl diphosphate; FTR, ferredoxin:thioredoxin reductase; MEcPP, 2-C-methyl-D-erythritol-2,4-cyclodiphosphate.

■ REFERENCES

- (1) Altincicek, B.; Duin, E. C.; Reichenberg, A.; Hedderich, R.; Kollas, A.-K.; Hintz, M.; Wagner, S.; Wiesner, J.; Beck, E.; and Jomaa, H.

- (2002) LytB protein catalyzes the terminal step of the 2-C-methyl-D-erythritol-4-phosphate pathway of isoprenoid biosynthesis. *FEBS Lett.* 532, 437–440.
- (2) Rohdich, F., Zepeck, F., Adam, P., Hecht, S., Kaiser, J., Laupitz, R., Gräwert, T., Amslinger, S., Eisenreich, W., Bacher, A., and Arigoni, D. (2003) The deoxyxylulose phosphate pathway of isoprenoid biosynthesis: Studies on the mechanisms of the reactions catalyzed by IspG and IspH protein. *Proc. Natl. Acad. Sci. U.S.A.* 100, 1586–1591.
- (3) Wolff, M., Seemann, M., Bui, B. T. S., Frapart, Y., Tritsch, D., Estrabot, A. G., Rodríguez-Concepción, M., Boronat, A., Marquet, A., and Rohmer, M. (2003) Isoprenoid biosynthesis via the methylerythritol phosphate pathway: The (E)-4-hydroxy-3-methylbut-2-enyl diphosphate reductase (LytB/IspH) from *Escherichia coli* is a [4Fe-4S] protein. *FEBS Lett.* 541, 115–120.
- (4) Rohmer, M. (1999) The discovery of a mevalonate-independent pathway for isoprenoid biosynthesis in bacteria, algae and higher plants. *Nat. Prod. Rep.* 16, 565–574.
- (5) Eisenreich, W., Bacher, A., Arigoni, D., and Rohdich, F. (2004) Biosynthesis of isoprenoids via the non-mevalonate pathway. *Cell. Mol. Life Sci.* 61, 1401–1426.
- (6) Rohdich, F., Bacher, A., and Eisenreich, W. (2005) Isoprenoid biosynthetic pathways as anti-infective drug targets. *Biochem. Soc. Trans.* 33, 785–791.
- (7) Jomaa, H., Wiesner, J., Sanderbrand, S., Altincicek, B., Weidemeyer, C., Hintz, M., Turbachova, I., Eberl, M., Zeidler, J., Lichtenthaler, H. K., Soldati, D., and Beck, E. (1999) Inhibitors of the nonmevalonate pathway of isoprenoid biosynthesis as antimalarial drugs. *Science* 285, 1573–1576.
- (8) Kuzuyama, T., Shimizu, T., Takahashi, S., and Seto, H. (1998) Direct formation of 2-C-methyl-D-erythritol 4-phosphate from 1-deoxy-D-xylulose 5-phosphate by 1-deoxy-D-xylulose 5-phosphate reductoisomerase, a new enzyme in the non-mevalonate pathway to isopentenyl diphosphate. *Tetrahedron Lett.* 39, 7913–7916.
- (9) Zeidler, J., Schwender, J., Müller, C., Wiesner, J., Weidemeyer, C., Beck, E., Jomaa, H., and Lichtenthaler, H. K. (1998) Inhibition of the non-mevalonate 1-deoxy-D-xylulose-5-phosphate pathway of plant isoprenoid biosynthesis by fosmidomycin. *Z. Naturforsch.* 53c, 980–986.
- (10) Koppisch, A. T., Fox, D. T., Blagg, B. S. J., and Poulter, D. C. (2002) *E. coli* MEP synthase: Steady-state kinetic analysis and substrate binding. *Biochemistry* 41, 236–243.
- (11) Missinou, M. A., Borrmann, S., Schindler, A., Issifou, S., Adegnika, A. A., Matsiegui, P.-B., Binder, R., Lell, B., Wiesner, J., Baranek, T., Jomaa, H., and Kremsner, P. G. (2002) Fosmidomycin for malaria. *Lancet* 360, 1941–1942.
- (12) Lell, B., Ruangweeraayut, R., Wiesner, J., Missinou, M. A., Schindler, A., Baranek, T., Hintz, M., Hutchinson, D., Jomaa, H., and Kremsner, P. G. (2003) Fosmidomycin, a novel chemotherapeutic agent for malaria. *Antimicrob. Agents Chemother.* 47, 735–738.
- (13) Borrmann, S., Issifou, S., Esser, G., Adegnika, A. A., Ramharther, M., Matsiegui, P. B., Oyakirome, S., Mawili-Mboumba, D. P., Missinou, M. A., Kun, J. F. J., Jomaa, H., and Kremsner, P. G. (2004) Fosmidomycin-clindamycin for the treatment of *Plasmodium falciparum* malaria. *J. Infect. Dis.* 190, 1534–1540.
- (14) Giessmann, D., Heidler, P., Haemers, T., Van Calenbergh, S., Reichenberg, A., Jomaa, H., Weidemeyer, C., Sanderbrand, S., Wiesner, J., and Link, A. (2008) Towards new antimalarial drugs: Synthesis of non-hydrolyzable phosphate mimics as feed for a predictive QSAR study on 1-deoxy-D-xylulose-5-phosphate reductoisomerase inhibitors. *Chem. Biodiversity* 5, 643–656.
- (15) Haemers, T., Wiesner, J., Giessmann, D., Verbrugghen, T., Hillaert, U., Ortmann, R., Jomaa, H., Link, A., Schlitzer, M., and Van Calenbergh, S. (2008) Synthesis of β - and γ -oxa isosteres of fosmidomycin and FR900098 as antimalarial candidates. *Bioorg. Med. Chem.* 16, 3361–3371.
- (16) Wiesner, J., Ortmann, R., Jomaa, H., and Schlitzer, M. (2007) Double ester prodrugs of FR900098 display enhanced In-Vitro antimalarial activity. *Arch. Pharm. (Weinheim, Ger.)* 340, 667–669.
- (17) Ortmann, R., Wiesner, J., Silber, K., Klebe, G., Jomaa, H., and Schlitzer, M. (2007) Novel deoxyxylulosephosphate-reductoisomerase inhibitors: Fosmidomycin derivatives with spacious acyl residues. *Arch. Pharm. (Weinheim, Ger.)* 340, 483–490.
- (18) Devreux, V., Wiesner, J., Jomaa, H., Van der Eycken, J., and Van Calenbergh, S. (2007) Synthesis and evaluation of α,β -unsaturated α -aryl-substituted fosmidomycin analogues as DXR inhibitors. *Bioorg. Med. Chem. Lett.* 17, 4920–4923.
- (19) Devreux, V., Wiesner, J., Jomaa, H., Rozenski, J., Van der Eycken, J., and Van Calenbergh, S. (2007) Divergent strategy for the synthesis of α -aryl-substituted fosmidomycin analogues. *J. Org. Chem.* 72, 3783–3789.
- (20) Haemers, T., Wiesner, J., Busson, R., Jomaa, H., and Van Calenbergh, S. (2006) Synthesis of α -aryl-substituted and conformationally restricted fosmidomycin analogues as promising antimalarials. *Eur. J. Org. Chem.*, 3856–3863.
- (21) Devreux, V., Wiesner, J., Goeman, J. L., Van der Eycken, J., Jomaa, H., and Van Calenbergh, S. (2006) Synthesis and biological evaluation of cyclopropyl analogues of fosmidomycin as potent *Plasmodium falciparum* growth inhibitors. *J. Med. Chem.* 49, 2656–2660.
- (22) Haemers, T., Wiesner, J., Van Poecke, S., Goeman, J., Henschker, D., Beck, E., Jomaa, H., and Van Calenbergh, S. (2006) Synthesis of α -substituted fosmidomycin analogues as highly potent *Plasmodium falciparum* growth inhibitors. *Bioorg. Med. Chem. Lett.* 16, 1888–1891.
- (23) Matthews, P. D., and Wurtzel, E. T. (2000) Metabolic engineering of carotenoid accumulation in *E. coli* by modulation of the isoprenoid precursor pool with expression of deoxyxylulose phosphate synthase. *Appl. Microbiol. Biotechnol.* 53, 396–400.
- (24) Rodríguez-Concepción, M., Querol, J., Lois, L. M., Imperial, S., and Boronat, A. (2003) Bioinformatic and molecular analysis of hydroxymethylbutenyl diphosphate synthase (GCPE) gene expression during carotenoid accumulation in ripening tomato fruit. *Planta* 217, 476–482.
- (25) Ajikumar, P. K., Xiao, W. H., Tyo, K. E. J., Wang, Y., Simeon, F., Leonard, E., Mucha, O., Phon, T. H., Pfeifer, B., and Stephanopoulos, G. (2010) Isoprenoid Pathway Optimization for Taxol Precursor Overproduction in *Escherichia coli*. *Science* 330, 70–74.
- (26) Lichtenthaler, H. K., Zeidler, J., Schwender, J., and Müller, C. (2000) The non-mevalonate isoprenoid biosynthesis of plants as a test system for new herbicides and drugs against pathogenic bacteria and the malaria parasite. *Z. Naturforsch.* 55c, 305–313.
- (27) Fellermeier, M., Kis, K., Sagner, S., Maier, U., Bacher, A., and Zenk, M. H. (1999) Cell-free conversion of 1-deoxy-D-xylulose 5-phosphate and 2-C-methyl-D-erythritol 4-phosphate into β -carotene in higher plants and its inhibition by fosmidomycin. *Tetrahedron Lett.* 40, 2743–2746.
- (28) Reikittke, I., Wiesner, J., Rohrich, R., Demmer, U., Warkentin, E., Xu, W. Y., Troschke, K., Hintz, M., No, J. H., Duin, E. C., Oldfield, E., Jomaa, H., and Ermler, U. (2008) Structure of (E)-4-hydroxy-3-methyl-but-2-enyl diphosphate reductase, the terminal enzyme of the non-mevalonate pathway. *J. Am. Chem. Soc.* 130, 17206–17207.
- (29) Gräwert, T., Rohdich, F., Span, I., Bacher, A., Eisenreich, W., Eppinger, J., and Groll, M. (2009) Structure of active IspH enzyme from *Escherichia coli* provides mechanistic insight into substrate reduction. *Angew. Chem., Int. Ed.* 48, 5756–5759.
- (30) Gräwert, T., Span, I., Eisenreich, W., Rohdich, F., Eppinger, J., Bacher, A., and Groll, M. (2010) Probing the reaction mechanism of IspH protein by X-ray structure analysis. *Proc. Natl. Acad. Sci. U.S.A.* 107, 1077–1081.
- (31) Gräwert, T., Span, I., Bacher, A., and Groll, M. (2010) Reductive Dehydroxylation of Allyl Alcohols by IspH Protein. *Angew. Chem., Int. Ed.* 49, 8802–8809.
- (32) Wang, W. X., Wang, K., Liu, Y. L., No, J. H., Li, J. K., Nilges, M. J., and Oldfield, E. (2010) Bioorganometallic mechanism of action, and inhibition, of IspH. *Proc. Natl. Acad. Sci. U.S.A.* 107, 4522–4527.
- (33) Wang, W. X., Li, J. K., Wang, K., Huang, C. C., Zhang, Y., and Oldfield, E. (2010) Organometallic mechanism of action and

inhibition of the 4Fe-4S isoprenoid biosynthesis protein GcpE (IspG). *Proc. Natl. Acad. Sci. U.S.A.* 107, 11189–11193.

(34) Gräwert, T., Kaiser, J., Zepeck, F., Laupitz, R., Hecht, S., Amslinger, S., Schramek, N., Schleicher, E., Weber, S., Haslbeck, M., Buchner, J., Rieder, C., Arigoni, D., Bacher, A., Eisenreich, W., and Rohdich, F. (2004) IspH protein of *Escherichia coli*: Studies on iron-sulfur cluster implementation and catalysis. *J. Am. Chem. Soc.* 126, 12847–12855.

(35) Zepeck, F., Gräwert, T., Kaiser, J., Schramek, N., Eisenreich, W., Bacher, A., and Rohdich, F. (2005) Biosynthesis of isoprenoids. Purification and properties of IspG protein from *Escherichia coli*. *J. Org. Chem.* 70, 9168–9174.

(36) Puan, K.-J., Wang, H., Dai, T., Kuzuyama, T., and Morita, C. T. (2005) *fldA* is an essential gene required in the 2-C-methyl-d-erythritol 4-phosphate pathway for isoprenoid biosynthesis. *FEBS Lett.* 579, 3802–3806.

(37) Wolff, M., Seemann, M., Grosdemange-Billiard, C., Tritsch, D., Campos, N., Rodríguez-Concepción, M., Boronat, A., and Rohmer, M. (2002) Isoprenoid biosynthesis via the methylerythritol phosphate pathway. (E)-4-Hydroxy-3-methylbut-2-enyl diphosphate: Chemical synthesis and formation from methylerythritol cyclodiphosphate by a cell-free system from *Escherichia coli*. *Tetrahedron* 43, 2555–2559.

(38) Röhrich, R. C., Englert, N., Troschke, K., Reichenberg, A., Hintz, M., Seeber, F., Balconi, E., Aliverti, A., Zanetti, G., Köhler, U., Pfeiffer, M., Beck, E., Jomaa, H., and Wiesner, J. (2005) Reconstitution of an apicoplast-localised electron transfer pathway involved in the isoprenoid biosynthesis of *Plasmodium falciparum*. *FEBS Lett.* 579, 6433–6438.

(39) Xiao, Y. L., Zhao, Z. K., and Liu, P. H. (2008) Mechanistic studies of IspH in the deoxyxylulose phosphate pathway: Heterolytic C-O bond cleavage at C-4 position. *J. Am. Chem. Soc.* 130, 2164–2165.

(40) Bradford, M. M. (1976) A rapid and sensitive method for the quantitation of microgram quantities of protein utilizing the principle of protein-dye binding. *Anal. Biochem.* 72, 248–254.

(41) Fish, W. W. (1988) Rapid colorimetric micromethod for the quantitation of complexed iron in biological sample. *Methods Enzymol.* 158, 357–364.

(42) Davoust, C. E., Doan, P. E., and Hoffman, B. M. (1996) Q-Band Pulsed Electron Spin-Echo Spectrometer and Its Application to ENDOR and ESEEM. *J. Magn. Reson., Ser. A* 119, 38–44.

(43) Zipse, H., Artin, E., Wnuk, S., Lohman, G. J. S., Martino, D., Griffin, R. G., Kacprzak, S., Kaupp, M., Hoffman, B., Bennati, M., Stubbe, J., and Lees, N. (2009) Structure of the nucleotide radical formed during reaction of CDP/TTP with the E441Q- $\alpha 2\beta 2$ of *E. coli* ribonucleotide reductase. *J. Am. Chem. Soc.* 131, 200–211.

(44) Hagen, W. R. (1992) EPR spectroscopy of iron-sulfur proteins. *Adv. Inorg. Chem.* 38, 165–222.

(45) Adam, P., Hecht, S., Eisenreich, W., Kaiser, J., Gräwert, T., Arigoni, D., Bacher, A., and Rohdich, F. (2005) Biosynthesis of terpenes: Studies on 1-hydroxy-2-methyl-2-(E)-butenyl 4-diphosphate reductase. *Proc. Natl. Acad. Sci. U.S.A.* 99, 12108–12113.

(46) Seemann, M., Janthawornpong, K., Schweizer, J., Bottger, L. H., Janoschka, A., Ahrens-Botzong, A., Tambou, M. N., Rotthaus, O., Trautwein, A. X., Rohmer, M., and Schunemann, V. (2009) Isoprenoid biosynthesis via the MEP pathway: *In vivo* Mössbauer spectroscopy identifies a [4Fe-4S]²⁺ center with unusual coordination sphere in the LytB protein. *J. Am. Chem. Soc.* 131, 13184–13185.

(47) Cammack, R., Patil, D. S., and Fernandez, V. M. (1985) Electron-spin-resonance/electron-paramagnetic-resonance spectroscopy of iron-sulphur enzymes. *Biochem. Soc. Trans.* 13, 572–578.

(48) Staples, C. R., Ameyibor, E., Fu, W., Gardet-Salvi, L., Stritt-Etter, A.-L., Schürmann, P., Knaff, D. B., and Johnson, M. K. (1996) The function and properties of the iron-sulfur center in spinach ferredoxin:thioredoxin reductase: A new biological role for iron-sulfur clusters. *Biochemistry* 35, 11425–11434.

(49) Staples, C. R., Gaymard, E., Stritt-Etter, A.-L., Telser, J., Hoffman, B. M., Schürmann, P., Knaff, D. B., and Johnson, M. K. (1998) Role of the [Fe₄S₄] cluster in mediating disulfide reduction in spinach ferredoxin:thioredoxin reductase. *Biochemistry* 37, 4612–4620.

(50) Dai, S., Schwendtmayer, C., Schürmann, P., Ramaswamy, S., and Eklund, H. (2000) Redox signaling in chloroplasts: Cleavage of disulfides by an iron-sulfur cluster. *Science* 287, 655–658.

(51) Jameson, G. N. L., Walters, E. M., Manieri, W., Schürmann, P., Johnson, M. K., and Huynh, B. H. (2003) Spectroscopic evidence for site specific chemistry at a unique iron site of the [4Fe-4S] cluster in ferredoxin:thioredoxin reductase. *J. Am. Chem. Soc.* 125, 1146–1147.

(52) Walters, E. M., Garcia-Serres, R., Jameson, G. N. L., Glauser, D. A., Bourquin, F., Manieri, W., Schürmann, P., Johnson, M. K., and Huynh, B.-H. (2005) Spectroscopic characterization of site-specific [Fe₄S₄] cluster chemistry in ferredoxin:thioredoxin reductase: Implications for the catalytic mechanism. *J. Am. Chem. Soc.* 127, 9612–9624.

(53) Wang, K., Wang, W. X., No, J. H., Zhang, Y. H., Zhang, Y., and Oldfield, E. (2010) Inhibition of the Fe₄S₄-Cluster-Containing Protein IspH (LytB): Electron Paramagnetic Resonance, Metallacycles, and Mechanisms. *J. Am. Chem. Soc.* 132, 6719–6727.

(54) Lee, H. I., Igarashi, R. Y., Laryukhin, M., Doan, P. E., Dos Santos, P. C., Dean, D. R., Seefeldt, L. C., and Hoffman, B. M. (2004) An organometallic intermediate during alkyne reduction by nitrogenase. *J. Am. Chem. Soc.* 126, 9563–9569.

(55) Shanmugam, M., Zhang, B., McNaughton, R. L., Kinney, R. A., Hille, R., and Hoffman, B. M. (2010) The Structure of Formaldehyde-Inhibited Xanthine Oxidase Determined by 35 GHz ²H ENDOR Spectroscopy. *J. Am. Chem. Soc.* 132, 14015–14017.

(56) Dai, S., Saarinen, M., Ramaswamy, S., Meyer, Y., Jacquot, J.-P., and Eklund, H. (1996) Crystal structure of *Arabidopsis thaliana* NADPH dependent thioredoxin reductase at 2.5 Å resolution. *J. Mol. Biol.* 264, 1044–1057.

(57) Walters, E. M., Garcia-Serres, R., Jameson, G. N. L., Glauser, D. A., Bourquin, F., Manieri, W., Schürmann, P., Johnson, M. K., and Huynh, B.-H. (2005) Spectroscopic characterization of site-specific [Fe₄S₄] cluster chemistry in ferredoxin:thioredoxin reductase: Implications for the catalytic mechanism. *J. Am. Chem. Soc.* 127, 9612–9624.

(58) Xu, W., Lees, N. S., Adedeji, D., Wiesner, J., Jomaa, H., Hoffman, B. M., and Duin, E. C. (2010) Paramagnetic Intermediates of (E)-4-Hydroxy-3-methylbut-2-enyl Diphosphate Synthase (GcpE/IspG) under Steady-State and Pre-Steady-State Conditions. *J. Am. Chem. Soc.* 132, 14509–14520.

(59) Mouesca, J. M., and Lamotte, B. (1998) Iron-sulfur clusters and their electronic and magnetic properties. *Coord. Chem. Rev.* 178, 1573–1614.

(60) Lepape, L., Lamotte, B., Mouesca, J. M., and Rius, G. (1997) Paramagnetic states of four iron four sulfur clusters. 1. EPR single-crystal study of 3+ and 1+ clusters of an asymmetrical model compound and general model for the interpretation of the g-tensors of these two redox states. *J. Am. Chem. Soc.* 119, 9757–9770.

(61) Wang, W., Wang, K., Li, J., Nellutla, S., Smirnova, T. I., and Oldfield, E. (2011) An ENDOR and HYSCORE Investigation of a Reaction Intermediate in IspG (GcpE) Catalysis. *J. Am. Chem. Soc.* 133, 8400–8403.

(62) Beinert, H., Kennedy, M. C., and Stout, C. D. (1996) Aconitase as iron-sulfur protein, enzyme, and iron-regulatory protein. *Chem. Rev.* 96, 2335–2373.